Supplementary Information

Structure-property relationships of epoxy functionalized enoate ester-based tailored hybrid gels-doped with different polysaccharides

Mertcan ER and Nermin ORAKDOGEN*

Istanbul Technical University, Department of Chemistry, Soft Materials Research Laboratory, 34469, Maslak, Istanbul, Turkey, Tel: +90-212-285-3305.
*Corresponding author; e-mail: orakdogen@itu.edu.tr

Synthesis protocol and structural parameters of enoate ester-based hybrid gels

Hybrid networks containing different types of natural polymer-based components; Hyaluronic acid (HyA), Dextrin (Dex), Maltodextrin (MDex), Carboxymethly cellulose (CMC) and Xanthan gum (XG) were prepared using difunctional hydrophilic crosslinker diethyleneglycol dimethacrylate (DEGDMA). Enoate ester-based hybrid gels containing different natural polymer-based substitutes (NPS) were synthesized via free radical crosslinking (cryo)polymerization of HEMA as neutral monomer and GMA as epoxy-functional hydrophobic comonomer.

Table S1. Synthesis protocol and structural parameters of hybrid PHG/NPS-gels containing different NPS.

HEMA content	80 mol%
GMA content	20 mol%
DEGDMA crosslinker	0.134 mM
Crosslinker ratio *X* (mole ratio of DEGDMA to HEMA+GMA)	1/74
APS content	3.51 mM
TEMED content	24.9 mM (0.375 v/v%)
NPS component	Bacteria origin: Hyaluronic Acid, Dextrin, Xanthan Gum Plant origin: Maltodextrin, Carboxymethyl Cellulose,
Polymerization temp.	24 °C, -18 °C

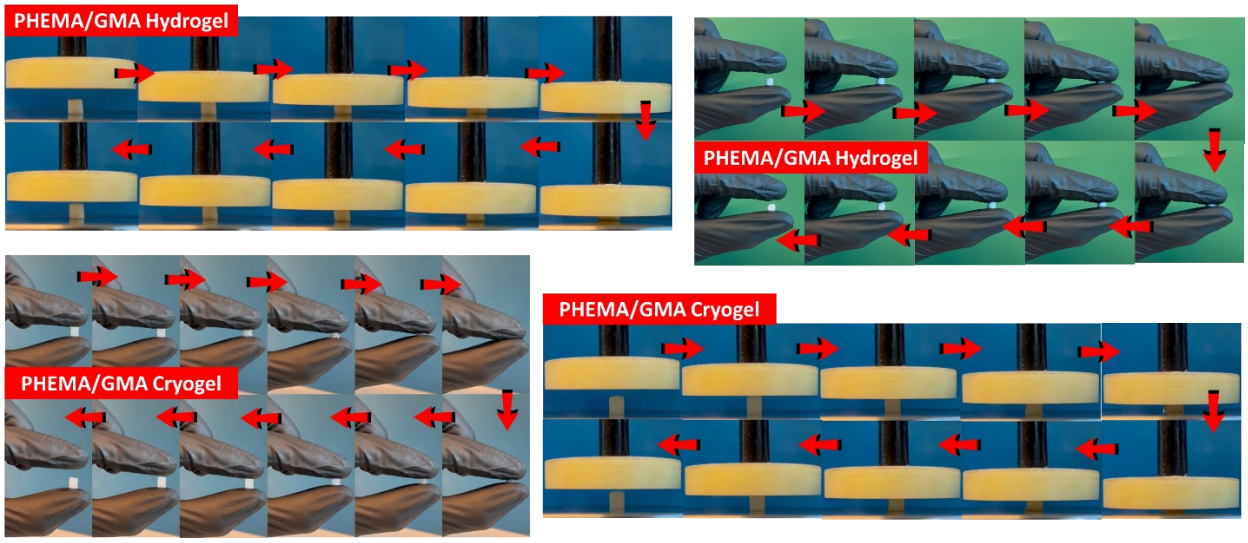

Figure S1. Optical images during finger-compression and uniaxial compression test of copolymer PHG hdyrogel and cryogel samples.

Solvent-induced swelling and solubility parameter of hybrid PHG/NPS gels

The swelling tendency of hybrid gels was evaluated using 16 different solvents with various solubility parameters; dichloromethane, N,N-dimethylformamide (DMF), acetone, ethylacetate, ethanol, methanol, hexane, dimethysulfoxide, acetonitrile, tetrahydrofuran (THF), 1,4-dioxane, 2-butanol, diethylether, 1,2-dichloroethane, cyclohexanone and acetic acid. Figure S2 presents the equilibrium volume swelling ratio φ_V of hybrid PHG/HyA cryogel samples containing Hyaluronic acid after equilibrium swelling in various solvents shown as a function of Hildebrand solubility parameter.

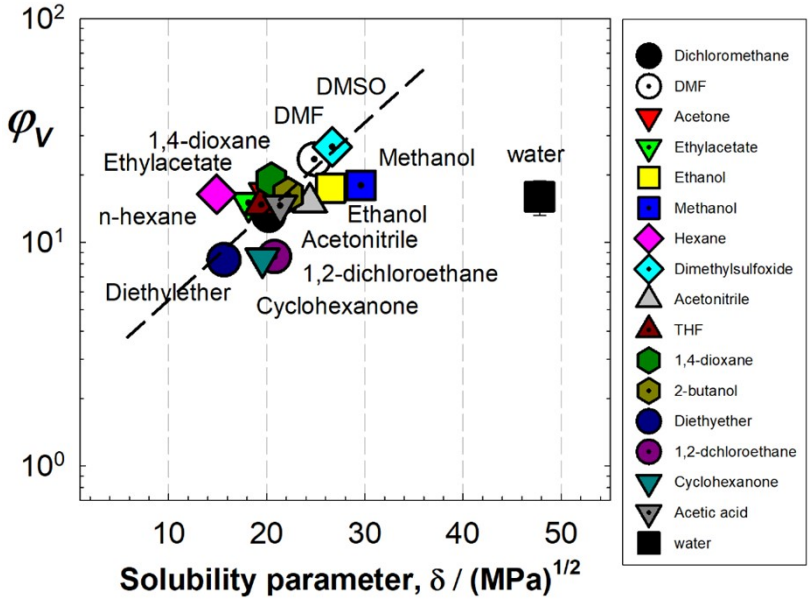

Figure S2. Equilibrium volume swelling ratio φ_V of hybrid PHG/HyA cryogel sample containing Hyaluronic acid after equilibrium swelling in various solvents shown as a function of Hildebrand solubility parameter.

Table S2. Hildebrand Solubility parameters of the solvents used in the swelling.

Solvent	δ_d $(MPa)^{1/2}$	δ_P $(MPa)^{1/2}$	δ_h $(MPa)^{1/2}$	$\delta_{overall}$ $(MPa)^{1/2}$
Dichloromethane	18.2	6.3	6.1	20.20
N,N-Dimethylformamide	17.4	13.7	11.3	24.86
Acetone	15.5	10.4	7.0	19.94
Ethyl Acetate	15.8	5.3	7.2	18.15
Ethanol	15.8	8.8	19.4	26.52
Methanol	15.1	12.3	22.3	29.61
Hexane	14.9	0.0	0.0	14.90
Dimethyl Sulfoxide	18.4	16.4	10.2	26.68
Acetonitrile	15.3	18.0	6.1	24.40
Tetrahydrofuran	16.8	5.7	8.0	19.46
1,4-Dioxane	19.0	1.8	7.4	20.47
2-Butanol	15.8	5.7	14.5	22.19
Diethyl Ether	14.5	2.9	5.1	15.64
1,2-Dichloroethane	19.0	7.4	4.1	20.80
Cyclohexanone	17.8	6.3	5.1	19.56
Acetic Acid	14.5	8.0	13.5	21.37

Table S3. Linearized forms of the kinetic models applied in the adsorption process.

Adsorption Kinetic Model	Linearized Equation	Plot	Kinetic parameters	Description of adsorption
Pseudo-First-order	$\ln(q_e - q_t) = \ln q_e - k_1 t$	$\ln(q_e - q_t)$ against t curves	k_1 is pseudo-first-order rate constant (min^{-1})	The slope and intercept of $\ln(q_e - q_t)$ against t curves give the values of k_1 and q_e
Pseudo-Second-order	$\frac{t}{q_t} = \frac{t}{q_e} + \frac{1}{k_2 q_e^2}$	t/q_t against t curves	k_2 is pseudo-second-order rate constant (g mg^{-1} min^{-1})	The values of k_2 and q_e are determined from the slope and intercept
Elovich	$q_t = \frac{1}{\beta}\ln t + \frac{1}{\beta}\ln(\alpha\beta)$	q_t against lnt curves	α is a constant for rate of chemisorption, β is a constant for extent of surface coverage of adsorbent	β, the number of remained sites after adsorption process, is determined from the slope and α is determined from the intercept.
Avrami	$\ln\left[\ln\left(\frac{q_e}{q_e - q_t}\right)\right] = n_{Av}\ln k_{Av} + n_{Av}\ln t$	$\ln(\ln(q_e/q_e - q_t))$ against lnt curves	k_{Av} is Avrami kinetic constant, and n_{Av} is Avrami exponent	Avrami exponent n_{Av} which is an indicator of the changes in the adsorption mechanism determined from the slope and the value of k_{Av} is determined from the intercept.
Fractional-power model	$\ln q_t = \ln k_{fr} + \nu_{fr}\ln t$	$\ln q_t$ against lnt curves	k_{fr} and ν_{fr} are the fractional power kinetic constants	ν_{fr} is determined from the slope and the value of k_{fr} is determined from the intercept.
Intraparticle diffusion model	$q_t = k_{diff} t^{1/2} + C$	q_t against $t^{1/2}$ plot	k_{diff} is rate constant for intraparticle diffusion (mg g^{-1} $min^{-1/2}$), and C is a constant for thickness of boundary layer.	k_{diff} is determined from the slope

Table S4. Linearized forms of the isotherm models applied in the adsorption.

Isotherm Model	Linearized Equation	Plot	Isotherm parameters	Description of Isotherm
Langmuir	$\frac{1}{q_e}=\frac{1}{q_{max}K_LC_e}+\frac{1}{q_{max}}$ $R_L=\frac{1}{1+K_LC_o}$	$1/q_e$ versus $1/C_e$ plot	q_{max} (mg g^{-1}) is maximum adsorption capacity of adsorbent, K_L (L/mg) is Langmuir adsorption constant, R_L is separation factor	R_L value shows that adsorption process is irreversible for R_L = 0, is favorable for 0 < R_L < 1, linear for R_L = 1 or unfavorable for R_L > 1
Freundlich	$\ln q_e=\ln K_F+(1/n_F)\ln C_e$	$\ln q_e$ versus $\ln C_e$ plot	K_F(mg/g) $(mg/L)^{-1/n}$ is Freundlich isotherm constant and n_F is adsorption intensity	n_F is heterogeneity factor and $1/n_F$ <1 confirms a cooperative adsorption.
Temkin	$q_e=B_T\ln K_T+B_T\ln C_e$ $B_T=\frac{RT}{b_T}$	q_e versus $\ln C_e$ plot	K_T (L/mg) is Temkin isotherm equilibrium binding constant, b_T (J/mol) is Temkin isotherm constant related to heat of adsorption	If b_T is positive, adsorption process would be exothermic
Dubinin-Radushkevich (D-R)	$\ln q_e=\ln q_{max}-\beta\varepsilon^2$ $\varepsilon=RT\ln(1+\frac{1}{C_e})$ $E=\frac{1}{(2\beta)^{1/2}}$	$\ln q_e$ versus ε^2 plot	ε (J/mol) is potential of Polanyi, E is the mean adsorption energy and β is D-R isotherm constant (mol^2 / J^2)	β can be calculated from the intercept of the plot. Nature of adsorption can be determined by E values. The values between 8 and 16 kJ/mol indicate a chemisorption, and the process is a physical adsorption with the values less than 8 kJ/mol.

Structural characterization of enoate ester-based hybrid gels

Enoate ester-based hybrid PHG/NPS-gels containing different NPS together with a control gel PHG without NPS, were prepared by free-radicalic mechanism. The infrared spectra were presented in Figure 1. FTIR spectrum of raw HyA sample and HyA-loaded hybrid PHG/HyA is shown in Fig.1(B). The ether bands are assigned at 1163 and 964 cm^{-1} and the latter band belongs to the asymmetrical out-of-phase ring vibration. Amide III (CN vibration and part of NH bending) was detected at 1371 cm^{-1} and symmetric stretching vibration of planar carboxyl groups C=O of HyA was observed at 1405 cm^{-1}. For FTIR spectrum of MDex and PHG/MDex gel in Fig.1(D), the signals at 1364 and 1429 cm^{-1} were due to C–H bending and C–H wagging, respectively. The appearance of the signal at 1646 cm^{-1} corresponded to the tightly bound water. The peaks at 1026 and 926 cm^{-1} are due to the C–O–C stretching vibrations. The peaks at 1458, 1422 and 1342 cm^{-1} are associated to H-C-OH bending vibrations, and the peak at ~1645 cm^{-1} is due to −OH bending mode of water molecules of hydration. The absorbance in the region lower than 1000 cm^{-1} is attributed to the stretching vibrations between bonded glucose units. The peaks at 1091 and 1148 cm^{-1} was due to the asymmetric stretching of the bridge C–O–C. In FTIR spectra of CMC and PHG/CMC gels in Fig. 2(A), the band at 1314 cm^{-1} was assigned to symmetrical deformation of CH_2 group. The peak at 1580 cm^{-1} was assigned to stretching vibration of carboxyl (COO^-) group while the peak at 1405 cm^{-1} was due to streaking vibration of carboxyl group in the form of salt (COONa). The bands appeared at 1055 and 1018 cm^{-1} due to C-O symmetric stretching of primary alcoholic $–CH_2OH$ stretching mode and CH_2 twisting vibrations, while the peak at 1079 cm^{-}

[1] represent the C–O–C stretching vibration. In FTIR spectra of XG and PHG/XG gels in Fig. 2(B), the peak at 1731 cm^{-1} was associated to free carboxylic acid or ester groups of XG. The peaks at 1594 cm^{-1} and 1414 cm^{-1} were due to C-O asymmetric stretching and C-O symmetric stretching of carboxylate anion. For PHG/XG gel, the OH band became broad, less intense and shifted to 3372 cm^{-1} indicating the gel formation.

Table S5. The peak locations observed with the respective peak assignments.

Band Locations (cm^{-1})	Band Assignments	Band Locations From Refs. (cm^{-1})	Refs.
3365	O-H Stretching (GMA)	3350	[1]
2998	C-H Stretching (GMA)	2994	[1]
2947	C-H Stretching (GMA)	2946	[1]
1724	C=O Stretching (Carbonyl)	1724	[1]
1141	C-O-C Stretching (Ester)	1140	[2]
1062	-C-O Stretching (Ester)	1056	[3]
910	C-O-C Asymmetric Stretching (Epoxy)	900	[4]
839	C-O-C Symmetric Stretching (Epoxy)	850	[4]
1256	C-O-C Symmetric Stretching (Epoxy)	1252	[1]
3370	O-H Stretching (HEMA)	3430	[5]
2940	CH2 Stretching (HEMA)	2946	[5]
2882	CH3 Stretching (HEMA)	2886	[5]
1386	CH2 Twist and Rock (HEMA)	1390	[5]

Thermal degradation behavior of enoate ester-based hybrid gels

The copolymer PHEMA/GMA denoted by PHG showed one-step degradation profile with the initial stage up to about 225 ^{o}C being attributed to the water evaporation. The weight loss of PHG began at about 225 °C and reached a maximum at 288 °C. There was a weight loss of 81.8% between 226.3 °C and 398.5 °C assigned to decomposition reactions on the ester side chain and beyond 400 °C up to 600 °C, the overall weight loss was 91.1% as a result of random chain scission. It was previously reported that the thermal degradation of homopolymer PGMA starts with endothermic depolymerization at about 250 °C and is accompanied by the exothermic isomerization of epoxy group to the carbonyl one at about 308 °C. In TGA curve of raw HyA, about 50.1% weight loss takes place in the temperature range of 216.2 – 363.8 °C, while it was 46.8% in hybrid PHG/HyA gel. The two main mechanisms for HyA degradation are enzymatic degradation by hyaluronidase and chemical degradation by oxidative stress. However, HyA has been reported to be more stable against enzymatic and oxidation degradation in three-dimensional cross-linked gel structures than its native, linear form. The thermogram of raw Dex and raw MDex which consist of mainly a-1,6-glucosidic linkage, showed two stages of weight loss. The initial mass loss of Dex (≈ 5.4%) between 25 and 250.4 ^{o}C, and MDex (≈ 18.6%) between 25 and 223.1 ^{o}C might be due to the moisture loss. MDex lost more mass during this phase compared to those of Dex, suggesting that MDex was not really anhydrous. The second weight loss region up to about 350 °C is due to the degradation of the polysaccharide backbone. Thermograms of raw CMC

indicates one stage of breakdown; an initial weight loss, up to192.2 °C (≈ 5.3%), attributed to the presence of adsorbed moisture and the decarboxylation of CMC and pyrolysis of cellulosic backbone (up to ≈ 314.1 °C). The percentage of mass loss in this temperature range is about 35.6%. In TGA curve of XG, the weight of hybrid sample continuously decreased with increasing temperature from 340 to 600 °C corresponding to the fragmentation of side chains of XG and the main copolymer substructure, which eventually leads to the formation of carbonaceous residues. PHG/NPS hybrid backbone showed the decomposition process comparatively, at higher temperature as compared to raw NPS. It is noteworthy that the residue at 600 °C for CMC is 58.1%, while for copolymer PHG, it is 8.3%.

Salt-induced swelling of hybrid PHG/NPS gels

Figure S3 shows the equilibrium volume swelling ratio φ_V of hybrid PHEMA/GMA-NPS hydrogels in NaCl (A) and KCl (B) solutions shown as a function of ionic strength of salt and hybrid composition.

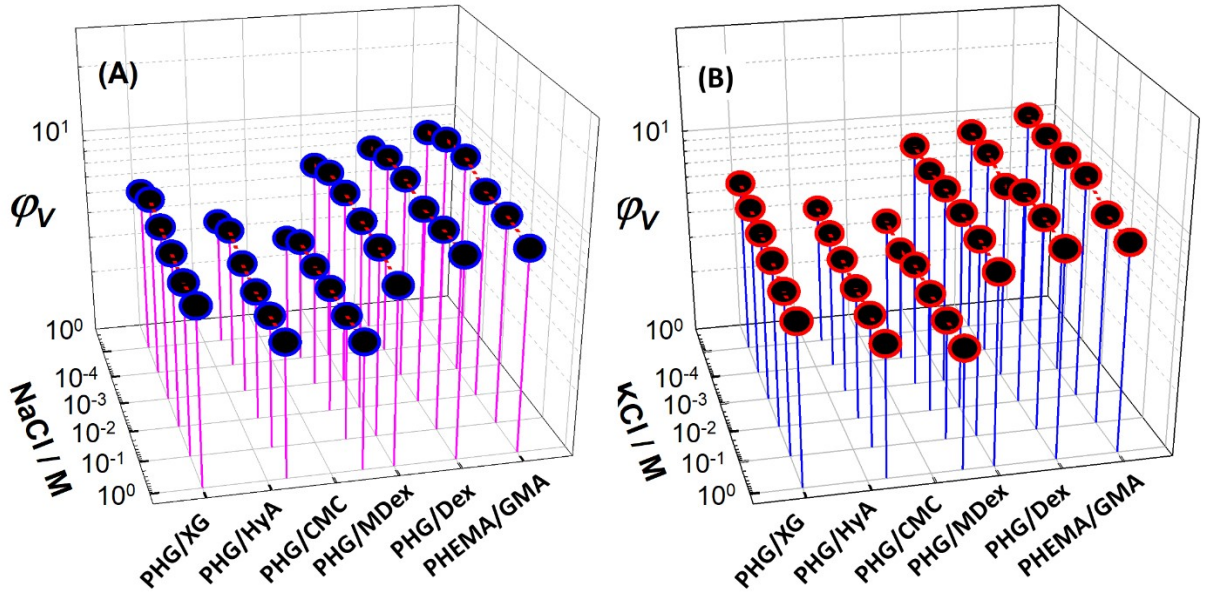

Figure S3. Equilibrium volume swelling ratio φ_V of hybrid PHEMA/GMA-NPS hydrogels in NaCl (A) and KCl (B) solutions shown as a function of ionic strength of salt and hybrid composition.

Adsorption properties of enoate ester-based hybrid gels

Figure S4 presents the adsorption capacity of hybrid PHG/NPS cryogels and hydrogels as a function of contact time.

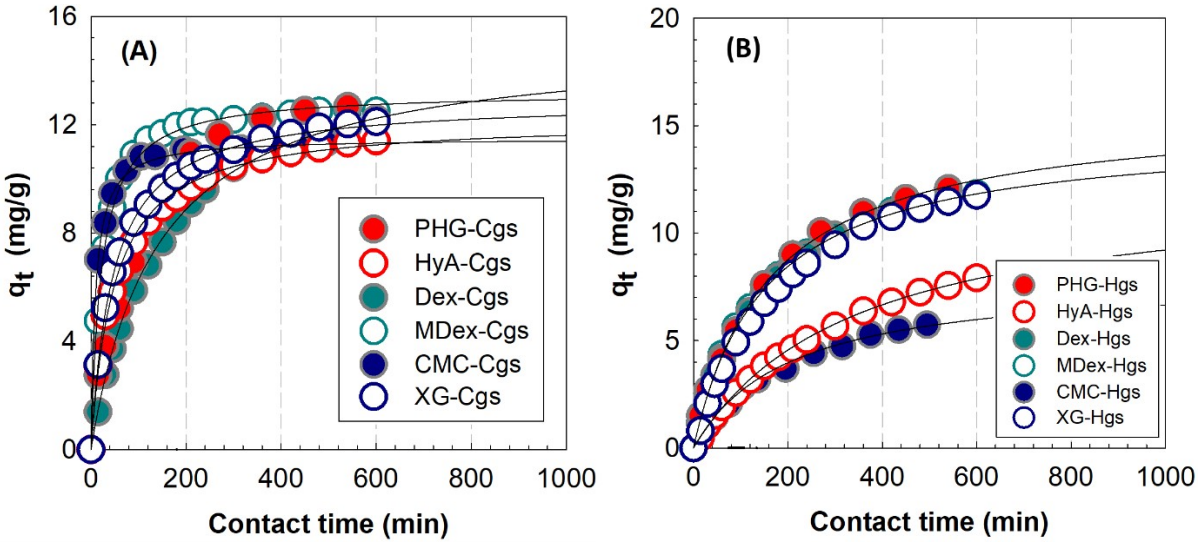

Figure S4. Adsorption capacity of hybrid PHG/NPS cryogels (A) and hydrogels (B) as a function of contact time.

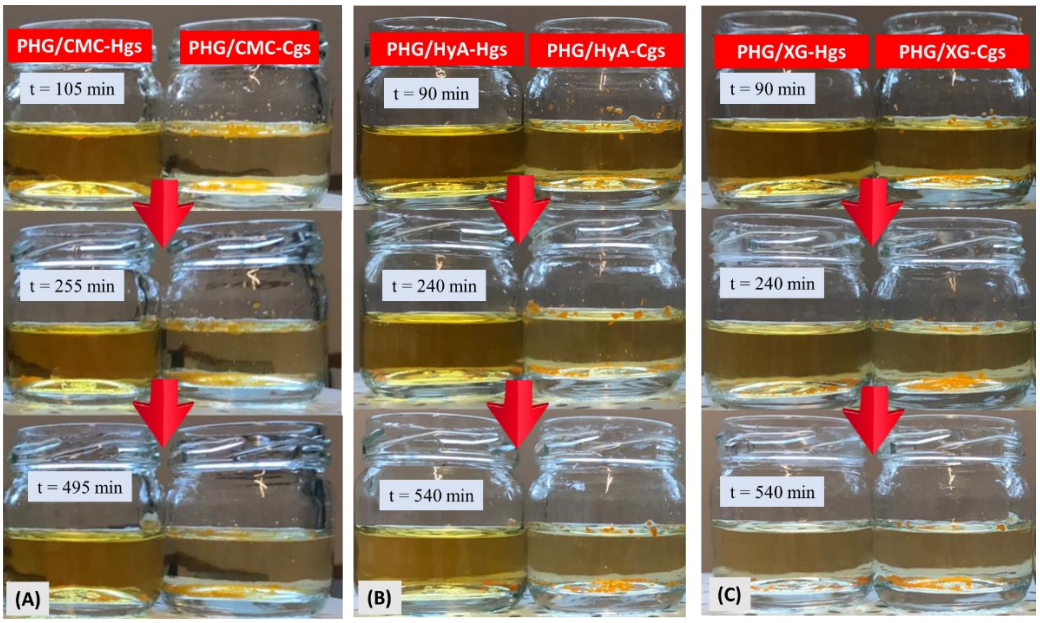

Fig. S5 Optical images of hybrid PHG/CMC (A), PHG/HyA (B) and PHG/XG (C) gels during the adsorption in aqueous MO solutions of 15 mg/L.

Fig. S6 presents dye adsorption kinetics of hybrid hydrogels fitted with Lagergren pseudo-first order kinetic model, Ho second order kinetic model, Avrami kinetic model and Elovich kinetic model. The solid line indicates the model-fit in the experimental data.

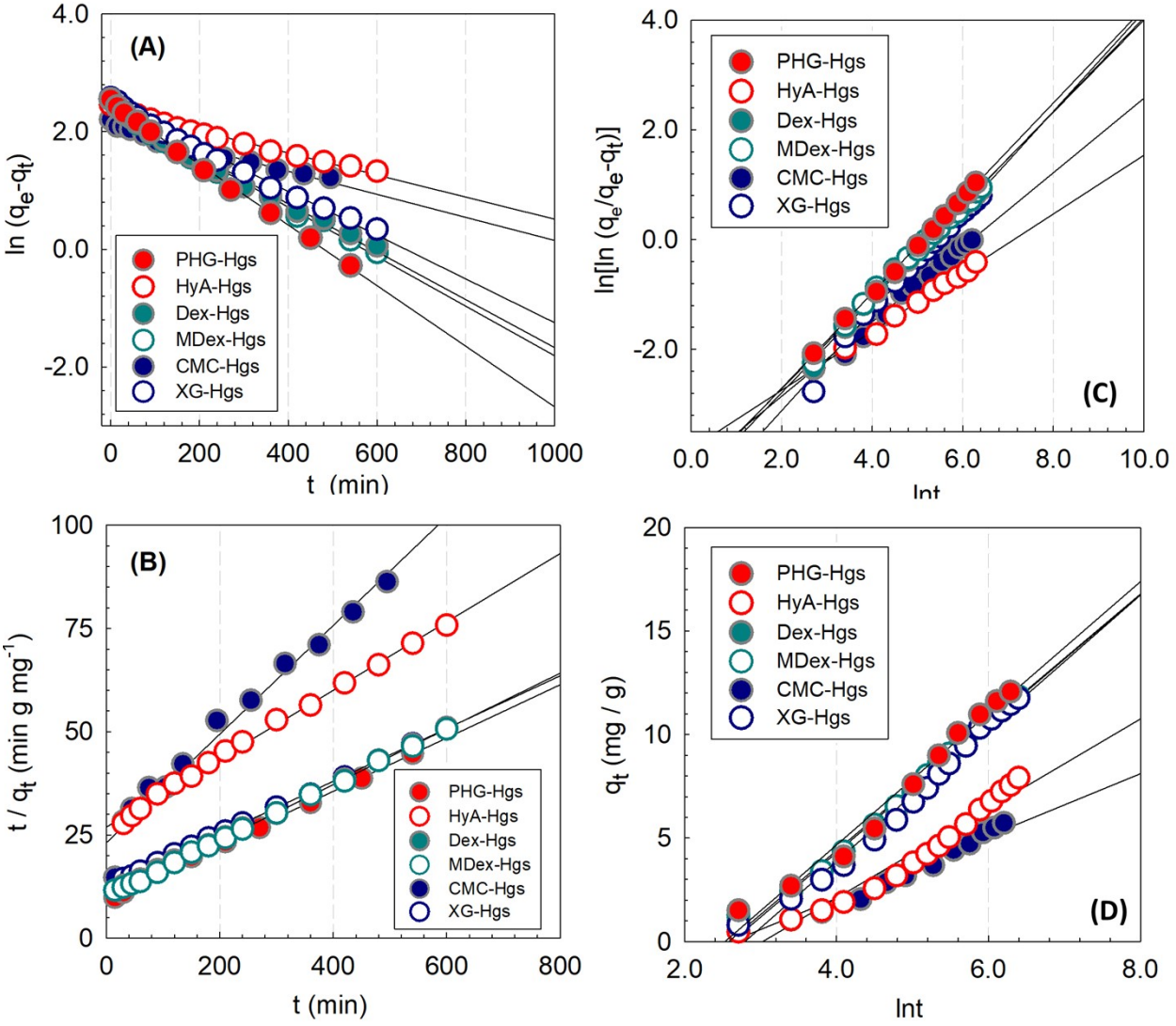

Fig. S6 (A) Dye adsorption kinetics of hybrid hydrogels fitted with Lagergren pseudo-first order kinetic model (A), Ho second order kinetic model (B), Avrami kinetic model (C) and Elovich kinetic model (D). The solid line indicates the model-fit in the experimental data.

Fig. S7 presents dye adsorption kinetics of hybrid PHG/NPS-Cgs and PHG/NPS-Hgs fitted with fractional power kinetic model. The solid lines correspond to the model-fit on the experimental data.

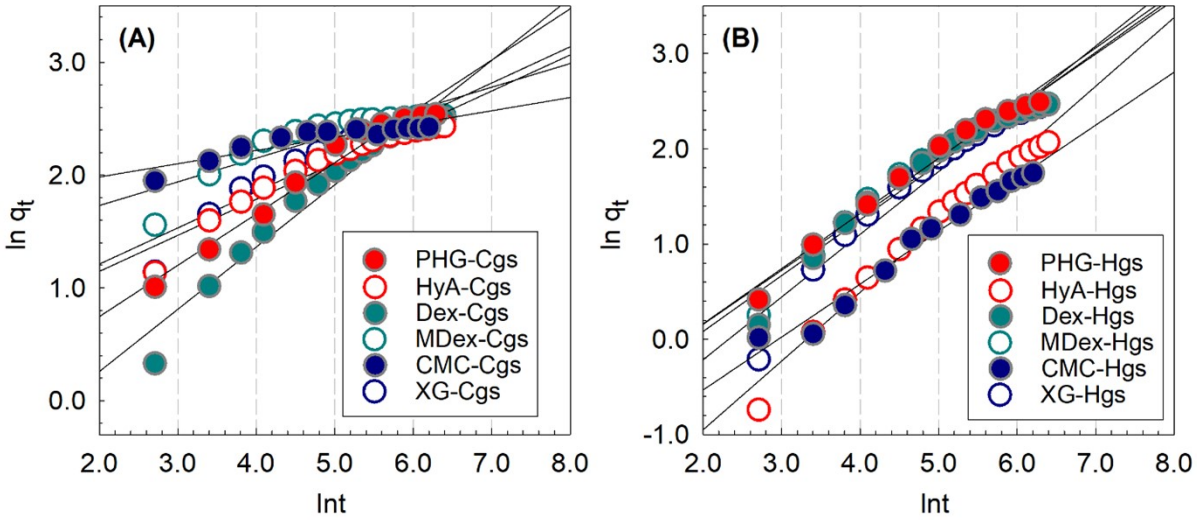

Fig. S7 Dye adsorption kinetics of hybrid PHG/NPS-Cgs (A) and PHG/NPS-Hgs (B) fitted with fractional power kinetic model. The solid lines correspond to the model-fit on the experimental data.

Table S6. Kinetic parameters of the pseudo-first-order, pseudo-second-order, Avrami kinetic, Elovich, fractional power model and intra-particle model for total MO dye sorption onto hybrid PHG/NPS hydrogels.

Pseudo-first order model			Elovich model		
PHG/NPS Hydrogels	$k_1 \times 10^{-2}$ (min^{-1})	R^2	α (mg/g min)	β (g/mg)	R^2
PHG	0.5153	0.9979	0.2530	0.3147	0.9802
PHG/HyA	0.1875	0.9875	0.1049	0.4628	0.9551
PHG/Dex	0.4881	0.9933	0.2270	0.3212	0.9906
PHG/MDex	0.4208	0.9908	0.2352	0.3232	0.9912
PHG/CMC	0.1956	0.9740	0.1107	0.6645	0.9507
PHG/XG	0.3717	0.9920	0.1970	0.3112	0.9853

Fractional power model				Avrami model		
PHG/NPS Hydrogels	ν_{fr} (min^{-1})	k_{fr} (mg /g)	R^2	n_{Av}	$k_{Av} \times 10^{-2}$ (min^{-1})	R^2
PHG	0.5792	0.1792	0.9784	0.8655	0.5938	0.9989
PHG/HyA	0.7213	0.0362	0.9793	0.5352	0.0803	0.9959
PHG/Dex	0.5859	0.1559	0.9520	0.8537	0.5156	0.9957
PHG/MDex	0.5675	0.1787	0.9557	0.8401	0.5331	0.9969
PHG/CMC	0.5975	0.0438	0.9820	0.6786	0.2021	0.9801
PHG/XG	0.6583	0.0978	0.9462	0.9090	0.4388	0.9903

Pseudo-second order model			Intra-particle model			
PHG/NPS Hydrogels	$k_2 \times 10^{-3}$ (min^{-1})	R^2	$k_{initial}$ (mg g^{-1} min$^{-1/2}$)	R^2	k_{later} (mg g^{-1} min$^{-1/2}$)	R^2
PHG	0.4239	0.9975	0.7116	0.9987	0.2939	0.9909
PHG/HyA	0.2545	0.9973	0.3710	0.9964	-	-
PHG/Dex	0.4345	0.9997	0.7277	0.9981	0.3385	0.9744
PHG/MDex	0.4445	0.9994	0.7591	0.9974	0.3027	0.9780
PHG/CMC	0.7477	0.9712	0.2782	0.9894	-	-
PHG/XG	0.3258	0.9995	0.6699	0.9977	0.3090	0.9711

Adsorption isotherms of enoate ester-based hybrid gels

Figure S8 shows the effect of initial concentration of MO dye on adsorption capacity and adsorption% of hybrid PHG/NPS hydrogels.

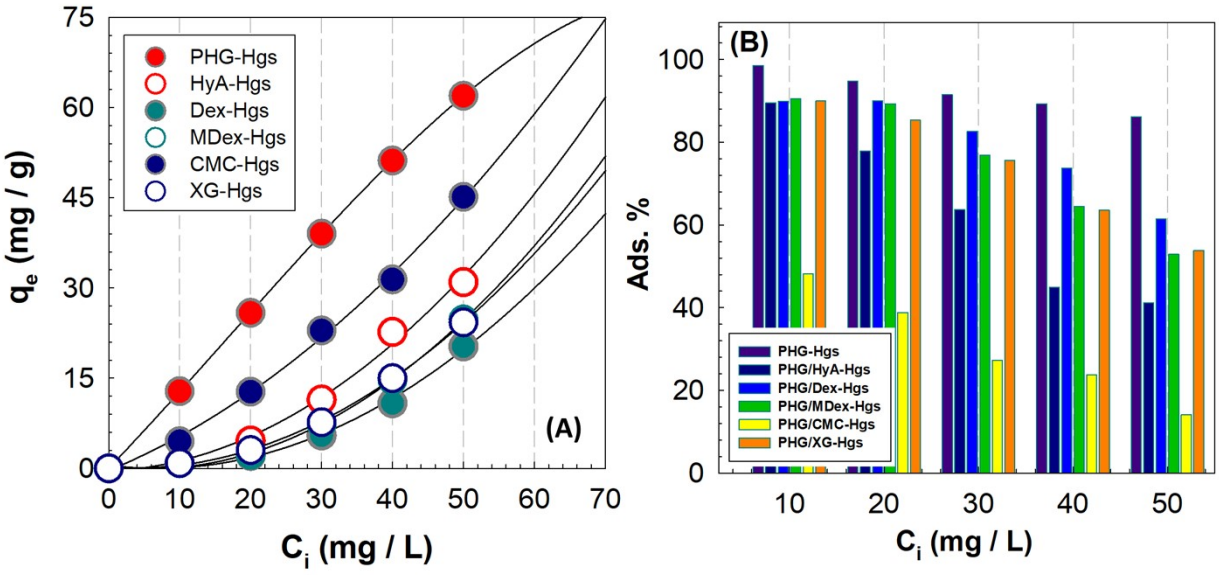

Figure S8. Effect of initial concentration of MO dye on adsorption capacity (A) and adsorption% (B) of hybrid PHG/NPS hydrogels.

Figure S9 shows the Langmuir, Freundlich, Dubinin-Radushkevich and Temkin isotherms for MO dye adsorption onto hybrid hydrogels, PHG/NPS-Hgs with different NPS-components.

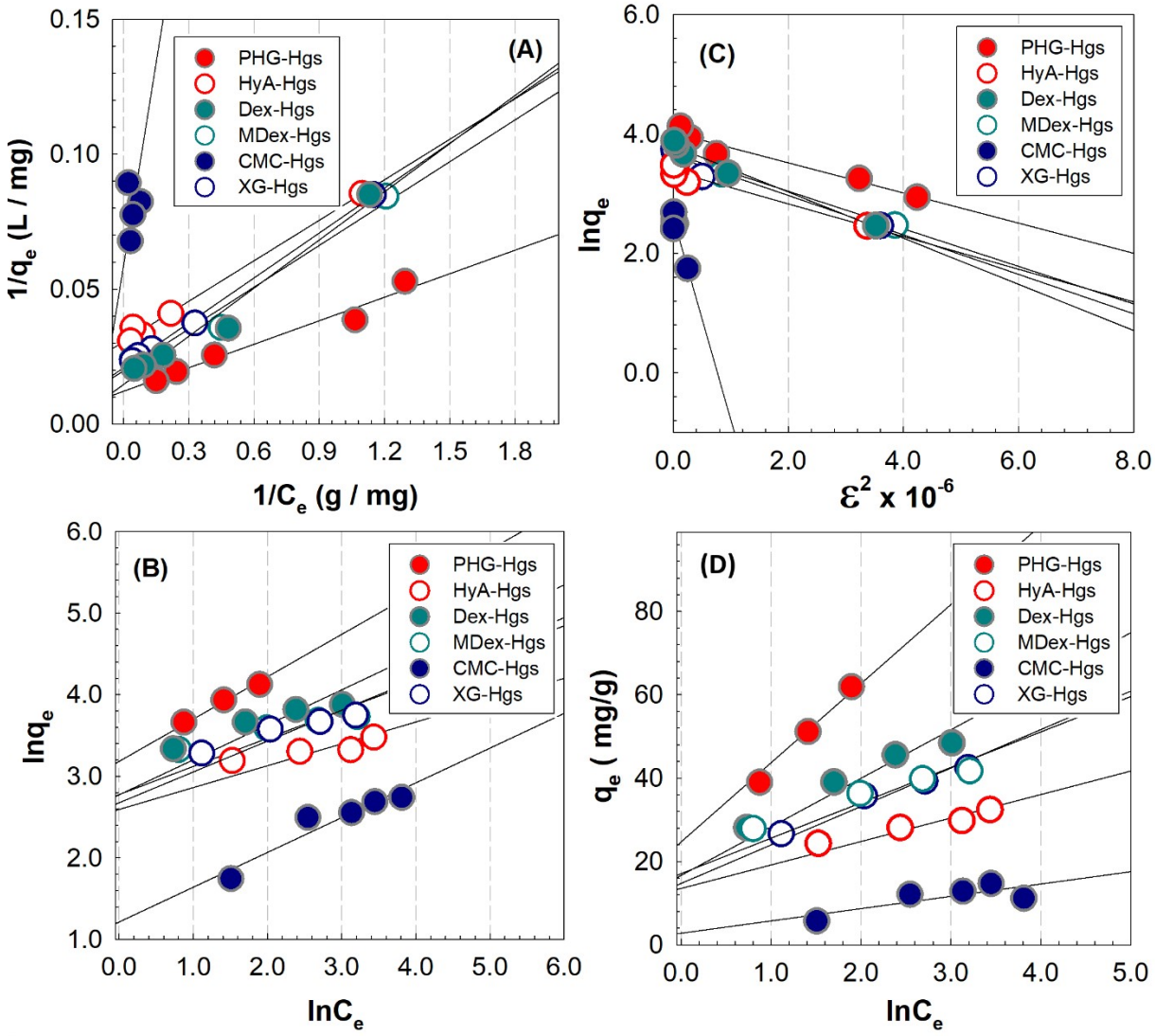

Figure S9. (A) Langmuir, (B) Freundlich (C) Dubinin-Radushkevich and (D) Temkin isotherms for MO dye adsorption onto hybrid hydrogels, PHG/NPS-Hgs with different NPS-components.

Table S7. Adsorption isotherm parameters for the adsorption of MO dye on hybrid hydrogels, PHG/NPS-Hgs containing different NPS.

		Hybrid PHG/NPS-Hydrogels					
Isotherm Model	**Isotherm Parameters**	**PHG**	**PHG/HyA**	**PHG/Dex**	**PHG/MDex**	**PHG/CMC**	**PHG/XG**
Langmuir	q_{max} (mg/L)	82.174	32.771	68.005	50.671	17.069	47.978
	K_L (L/mg)	0.4190	0.6102	0.2473	0.3821	0.1171	0.3755
	R_L	0.1926-0.0455	0.1408-0.0317	0.2879-0.0748	0.2073-0.0497	0.4605-0.1458	0.2102-0.0505
	R^2	0.9653	0.9926	0.9718	0.9755	0.9057	0.9986
Freundlich	K_F (mg/g)(mg/L)$^{-1/n}$	24.121	13.534	16.015	15.297	4.1263	14.519
	n_F	1.9272	3.6745	2.3324	2.9028	2.9994	2.6445
	R^2	0.9730	0.8774	0.8599	0.8402	0.6653	0.9133
Temkin	K_T (L/mg)	3.6800	14375.1	644.60	2746.07	70.202	1182.3
	b_T	130.51	9104.0	5778.7	7191.9	7431.3	6551.8
	R^2	0.9894	0.9029	0.9557	0.9304	0.6173	0.9778
D-R	β (mol^2/J^2)	0.2523	0.2733	0.3862	0.3142	3.3775	0.33012
	E (J/mol)	1.4076	1.3524	1.1377	1.2614	0.3847	1.2306
	R^2	0.9482	0.9573	0.9828	0.9883	0.9218	0.9529

Table S8. Band assignments for the FTIR spectrum of Methyl Orange dye.

Band Locations (cm^{-1})	Band Assignments	Band Locations From Refs. (cm^{-1})	Refs.
1598	-N=N- Stretching	1600	[6]
1515	-N=N- Stretching	1516	[6]
1361	-C-N Stretching	1361	[6]
1182	-C-N Stretching	1184	[6]
1112	-S=O Stretching	1111	[6]
1035	C-H Stretching (Benzene Skeleton)	1031	[6]
943	C-H Stretching (Benzene Skeleton)	939	[6]
692	C-H Stretching (Benzene Skeleton)	690	[6]
846	C-H Out-of-Plane Bending (Benzene Skeleton)	847.6	[7]
815	C-H Out-of-Plane Bending (Benzene Skeleton)	817.7	[7]
2898	-CH_3 Stretching	2901.4	[7]
2821	-CH_3 Stretching	2817.2	[7]
1361	-CH_3 Stretching	1366.1	[7]

Figure S10 presents the optical images of hybrid PHG/NPS Hgs and Cgs after adsorption in aqueous MO solutions with C_i = 20-50 mg/L.

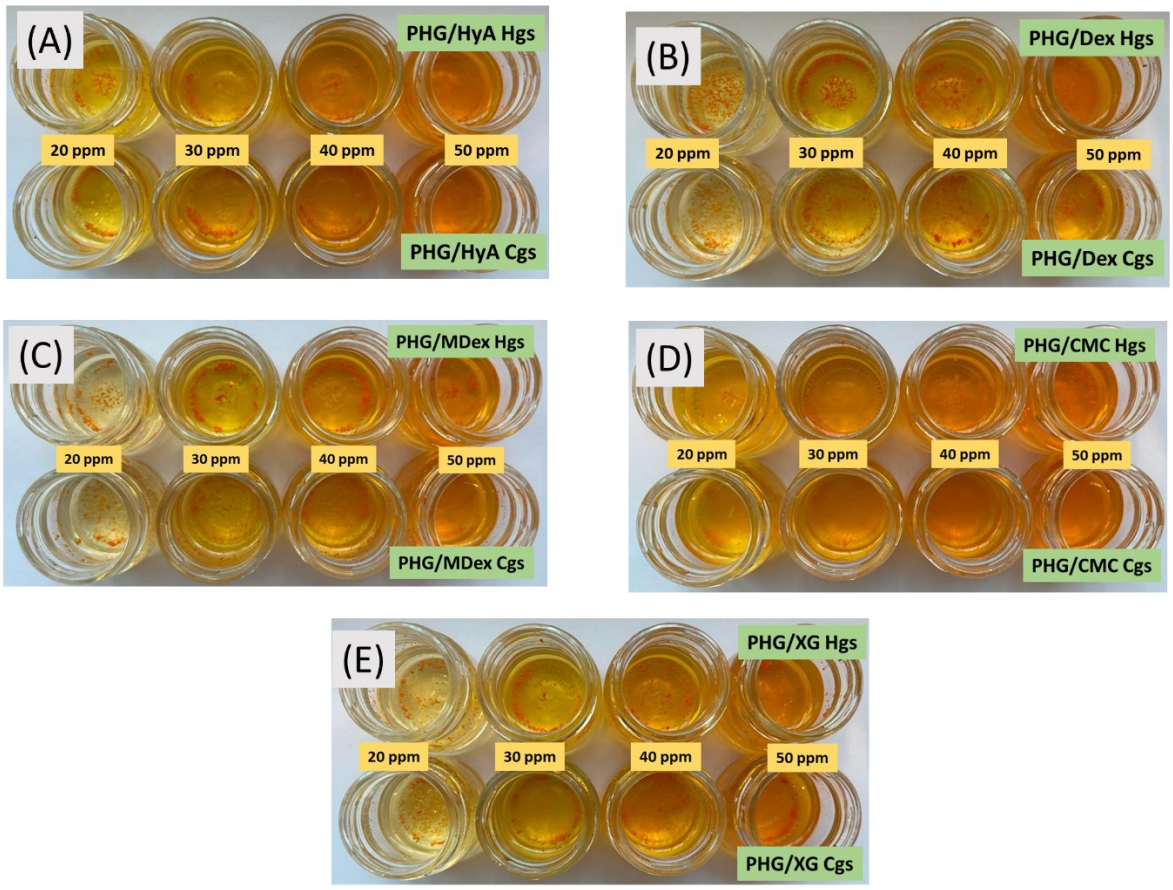

Figure S10. Optical images of hybrid PHG/NPS Hgs and Cgs after adsorption in aqueous MO solutions with C_i = 20-50 mg/L.

REFERENCES

[1] M. Faria, C. Vilela, F. Mohammadkazemi, A.J. Silvestre, C.S. Freire, N. Cordeiro, (2019). Poly (glycidyl methacrylate)/bacterial cellulose nanocomposites: Preparation, characterization and post-modification. International Journal of Biological Macromolecules, 127, 618-627. doi:10.1016/j.ijbiomac.2019.01.133

[2] S. Yuan, J. Zhang, Z. Yang, S. Tang, B. Liang, S.O. Pehkonen, (2017). Click functionalization of poly (glycidyl methacrylate) microspheres with triazole-4-carboxylic acid for the effective adsorption of Pb (II) ions. New Journal of Chemistry, 41(14), 6475-6488. doi:10.1039/C7NJ00797C

[3] P. Li, R. Xu, W. Wang, X. Li, Z. Xu, K.W. Yeung, P.K. Chu, (2013). Thermosensitive poly (N-isopropylacrylamide-co-glycidyl methacrylate) microgels for controlled drug release. Colloids and Surfaces B: Biointerfaces, 101, 251-255. doi:10.1016/j.colsurfb.2012.07.009

[4] K. Erol, L. Uzun, (2017). Two-step polymerization approach for synthesis of macroporous surface ion-imprinted cryogels. Journal of Macromolecular Science, Part A, 54(11), 867-875. doi:10.1080/10601325.2017.1342519

[5] H. Macková, Z. Plichta, H. Hlídková, O. Sedláček, R. Konefal, Z. Sadakbayeva, M. Dušková-Smrčková, D. Horák, S. Kubinová, (2017). Reductively Degradable Poly(2-hydroxyethyl methacrylate) Hydrogels with Oriented Porosity for Tissue Engineering Applications. ACS Applied Materials & Interfaces, 9(12), 10544-10553. doi:10.1021/acsami.7b01513

[6] N. Cyril, J.B. George, L. Joseph, V.P. Sylas, (2019). Catalytic degradation of methyl orange and selective sensing of mercury ion in aqueous solutions using green synthesized silver nanoparticles from the seeds of Derris trifoliata. Journal of Cluster Science, 30(2), 459-468. doi:10.1007/s10876-019-01508-9.

[7] L. Wu, X. Liu, G. Lv, R. Zhu, L. Tian, M. Liu, Y. Li, W. Rao, T. Liu, L. Liao, (2021). Study on the adsorption properties of methyl orange by natural one-dimensional nano-mineral materials with different structures. Scientific reports, 11(1), 1-11. doi:10.1038/s41598-021-90235-1